Laser-Driven Magnetic-Flux Compression in High-Energy-Density Plasmas

Citation: Gotchev, O. V. et al. "Laser-Driven Magnetic-Flux Compression in High-Energy-Density Plasmas." Physical Review Letters 103.21 (2009): 215004. © 2009 The American Physical Society

As Published: http://dx.doi.org/10.1103/PhysRevLett.103.215004

Publisher: American Physical Society

Persistent URL: http://hdl.handle.net/1721.1/52471

Version: Final published version: final published article, as it appeared in a journal, conference proceedings, or other formally published context

Laser-Driven Magnetic-Flux Compression in High-Energy-Density Plasmas

O. V. Gotchev,[1,2,3] P. Y. Chang,[1,2,4] J. P. Knauer,[1,2] D. D. Meyerhofer,[1,2,3,4] O. Polomarov,[1,2,3] J. Frenje,[2,5] C. K. Li,[2,5] M. J.-E. Manuel,[2,5] R. D. Petrasso,[2,5] J. R. Rygg,[6] F. H. Séguin,[2,5] and R. Betti[1,2,3,4]

[1]*Laboratory for Laser Energetics, University of Rochester, 250 East River Road, Rochester, New York 14623, USA*
[2]*Fusion Science Center for Extreme States of Matter, University of Rochester, 250 East River Road, Rochester, New York 14623, USA*
[3]*Department of Mechanical Engineering, University of Rochester, Rochester, New York 14627, USA*
[4]*Department of Physics and Astronomy, University of Rochester, Rochester, New York 14627, USA*
[5]*Plasma Science and Fusion Center, MIT, Cambridge, Massachusetts, USA*
[6]*Lawrence Livermore National Laboratory, Livermore, California, USA*

(Received 15 May 2009; published 18 November 2009)

The demonstration of magnetic field compression to many tens of megagauss in cylindrical implosions of inertial confinement fusion targets is reported for the first time. The OMEGA laser [T. R. Boehly *et al.*, Opt. Commun. **133**, 495 (1997)] was used to implode cylindrical CH targets filled with deuterium gas and seeded with a strong external field (>50 kG) from a specially developed magnetic pulse generator. This seed field was trapped (frozen) in the shock-heated gas fill and compressed by the imploding shell at a high implosion velocity, minimizing the effect of resistive flux diffusion. The magnetic fields in the compressed core were probed via proton deflectrometry using the fusion products from an imploding D_3He target. Line-averaged magnetic fields between 30 and 40 MG were observed.

DOI: 10.1103/PhysRevLett.103.215004 PACS numbers: 52.57.−z, 52.25.Xz, 52.55.Lf

In the magnetic fusion energy (MFE) concept, a strong magnetic field confines the plasma and reduces the electron thermal conduction to the vessel wall [1]. The magnetic pressure of typical ~0.1-MG fields is higher than the total energy density of the plasma (with $\beta = 2\mu_0 p/B^2 < 1$). MFE plasmas are fully magnetized and characterized by a Hall parameter $\omega_{ce}\tau > 1$ since the modest gyrofrequency ω_{ce} is matched by long collision times τ. In contrast, typical inertial confinement fusion (ICF) plasmas have collision frequencies higher by 10 to 12 orders of magnitude because of their extreme density. In such systems, thermal conduction losses are a major factor in the energy balance of an implosion. While it can be more difficult, magnetizing the hot spot in ICF implosions can lead to improved gains and to a reduction of the energy required for ignition. A similar approach is used in the magnetized target fusion concept [2], where the fusion burn requires relatively low-implosion velocities, provided there is an adequate magnetic thermal insulation. In ICF implosions, lower implosion velocities lead to higher gains [3]. However, tens of MG are needed to achieve $\omega_{ce}\tau \sim 1$ in the hot spot of a typical, direct drive DT ignition target [4] with hot-spot density of ~30 g/cc and a temperature of ~7 keV. Such a field is higher than both the self-generated magnetic fields (see Ref. [5]) and the external fields that can be generated by coils. Magnetic-flux compression [6] is a viable path to generating tens of MG magnetic fields with adequate size compression of a metal liner driven by high explosives [7,8] or by pulsed power. The latter approach has been pursued by the *Z*-pinch [9] communities. The results from the first experiments on a new approach that provides very effective flux compression are reported here. The field is compressed by the ablative pressure exerted on an imploding ICF capsule by the driving laser [10]. This approach was proposed in the 1980s [11] as a way to achieve record compressed fields with possible applications for fusion [12] but no laser experiments were performed. There are numerous advantages to this approach as the implosion velocity is high (a few 10^7 cm/s) and the hot plasma is an effective conductor that traps the embedded (seeded) initial magnetic field with minimal resistive diffusion. This approach can be used to magnetize high-energy-density plasmas for a number of applications ranging from controlled fusion to laboratory astrophysics.

Figure 1 describes cylindrical implosions on OMEGA that use axial seed fields embedded in the target prior to compression by the OMEGA laser [13]. The target was a

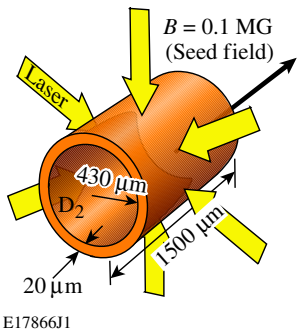

FIG. 1 (color online). Laser-driven flux compression in a cylindrical target. A plastic cylinder with a radius of 430 μm and wall thickness of 20 μm is filled with 9 atm of D_2 gas. The seed field is trapped by an ionization front created by the propagation of a strong shock wave in the gas.

20-μm-thick, 0.8-mm-diam CH cylindrical shell filled with D_2 gas. Some of the physical details of this concept are described in Ref. [10]. The shock-heated D_2 fuel traps the seed magnetic field, which would otherwise diffuse much faster through the relatively cold (resistive) imploding shell. The seed field was provided by a Helmholtz-like double coil [Fig. 2(a), coil diameter and separation are both 4 mm], coaxial with the cylindrical target [14]. A portable capacitive discharge system [14] delivers up to 80-kA current to the coils. The on-axis seed field was 50 to 90 kG at the target and 120 to 160 kG in the coil planes because of the coil separation chosen to avoid obscuring laser beams.

The compressed fields within the dense, optically thick ICF plasmas are difficult to measure. Proton deflectometry based on the method described in Refs. [15–17] is a viable diagnostic that has been implemented on OMEGA. A monoenergetic ($\Delta E/E \sim 0.03$), pointlike (size/object distance $\sim$0.01), time-gated (an $\sim$150-ps burst) proton source is provided by a glass sphere, filled with D-^{3}He gas mixture and driven by 20 OMEGA beams with a focal diameter of 300 μm [15]. The 14.7-MeV protons produced by the D-^{3}He fusion reactions are accelerated to $\sim$15.2 MeV by the charging of the backlighter target, and recorded on a CR-39 nuclear track detector which allows for both spatial and energy resolution (via the track diameter) of the particles incident on the surface [18]. The data [Fig. 2(b)] were generated as a convolution in space (source size, scattering at the object and detector) and time (finite duration) of the proton burst interacting with the field and target structure. None of the radial striations reported in Ref. [16] for spherical implosions was seen around the compressed core in these experiments, possibly because the target was imaged more than a nanosecond after the laser was turned off. A proton backlighter target yield of 3×10^7 would give a proton flux of 0.3 protons per μm^2 at the target and 20 000 protons per cm^2 at the detector.

A discrimination of tracks by energy (track diameter) was implemented to separate the core- (strong-field) traversing protons from the background, "free-space" particles that land in the same area of the detector. This is shown in Fig. 2(c), where the proton density map for shot 51069 [Fig. 2(b)] was used to construct two lineouts by taking a band of data and averaging over its width. The second curve in Fig. 2(c) is from tracks with only energy $E_k <$ 14.8 MeV caused by an additional slowdown through the magnetized target. It shows an asymmetric peak in the proton density caused by deflection in the target field. In contrast, the data from multiple "null" experiments performed to establish the particle-density pattern for implosions with no seed field, retain central symmetry in the cross-core lineouts (Fig. 3); i.e., the low-energy peak lines up with the trough of the high-energy proton lineout.

A simulation package based on the Monte Carlo particle-transport framework GEANT4 [19] was developed to predict and interpret the experimental data. After including the field topology and material parameters predicted by the LILAC-magnetohydrodynamic (MHD) code [20] for the time of proton probing, the particle-transport code computes the deflection pattern under the combined action of the field and scattering or energy loss processes. A comparison (Fig. 4) of the simulation predictions (solid line) and experimental data (dotted line) for shot 49704 in which a compressed field of 13 MG was predicted by the hydrocode, shows very good agreement in both the total fluence and low-energy-band lineouts. In Fig. 4(b), only the protons that had an incident energy lower than 14.8 MeV were included. The target in shot 49704 had a seed field of -10 kG and was probed relatively early in the implosion. In later experiments, where proton emission occurred at or near peak compression, the experimental lineouts at intermediate energies exhibited a double-

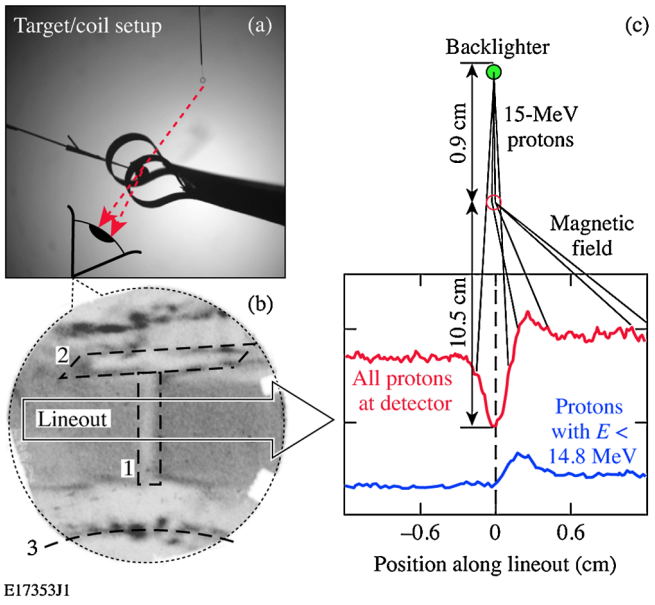

FIG. 2 (color online). (a) Photo of the target-coil setup. (b) Proton density map for shot 51069. Darker areas represent higher fluence: (1) compressed core, (2) target plug, and (3) coil shadow. (c) Lineouts in two energy bands expose the deflected protons.

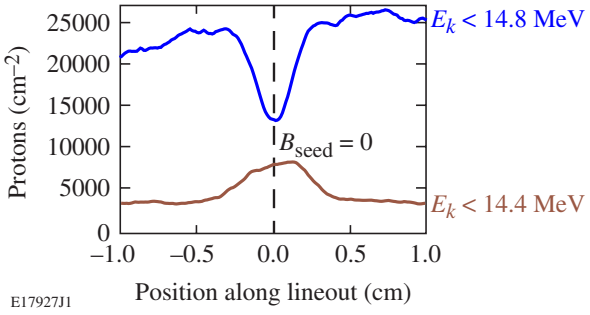

FIG. 3 (color online). (a) Cross-core lineouts from proton radiograph of shot 49693—an implosion with no external magnetic field—show that the core-traversing protons remained undeflected.

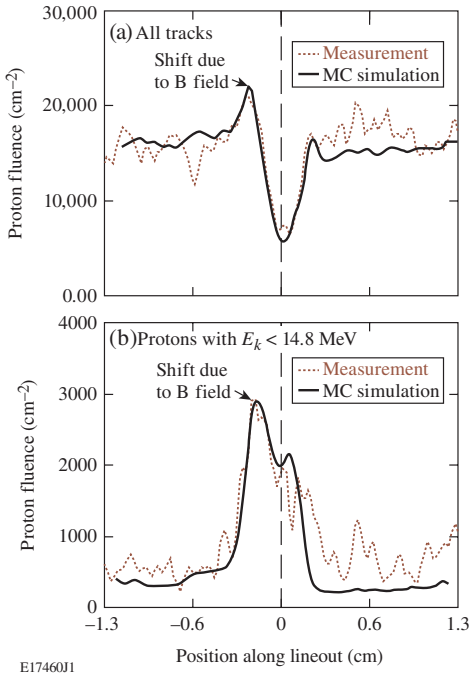

FIG. 4 (color online). Direct comparisons of measured (dotted line) and simulated (solid line) proton density lineouts across the core in shot 49704. (a) All protons; (b) protons intercepting the target (isolated by track diameter).

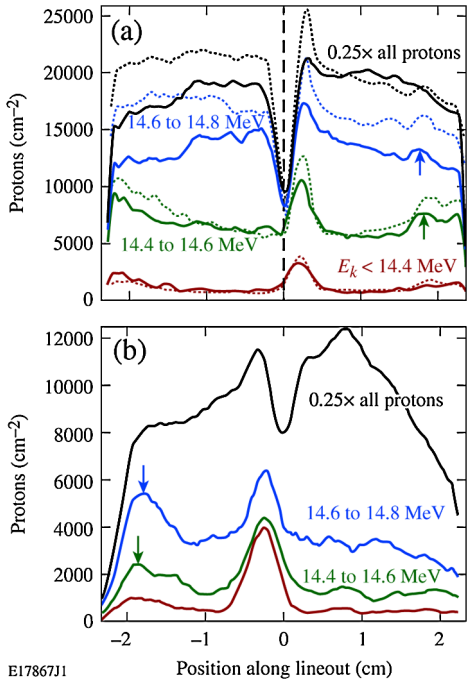

FIG. 5 (color online). (a) Partitioning of the data (solid lineouts) for shot 51069 in energy bands exposed the protons (deflected to the right) that traverse the high field in the target center. Energy band partitions in the Monte Carlo simulation are shown as dotted lineouts and match the compressed field ~30 MG. (b) Shot 52532 with the polarity of the seed field reversed shows a deflection to the left. Total and reduced-energy-band lineouts show large deflection matching a compressed field >36 MG.

deflection pattern with a second deflection peak farther from the center (indicated by the arrows in Fig. 5, shot 51069). This was first seen in Monte Carlo simulations, shown as dotted lines in Fig. 5(a), and was caused by an abrupt jump of the field in the small volume of the hot spot from much lower values in the shell (responsible for the first deflection). Early in time, at low compressed field, these two peaks were essentially merged as is the case with shot 49704. A comparison of the data for shot 51069, which had a 56-kG seed field, and the simulation shows good qualitative agreement, capturing the double-peak-deflection pattern. The protons that were slowed down the most (bottom curve) were those that crossed through the shell but not the hot spot, missing the peak field. From a second peak deflection of 1.9 ± 0.1 cm, one can estimate an average product $\langle R_B B_{\max} \rangle \approx 2(\theta)(m_p v_p/e)c$ or 0.052 MG cm, corresponding to an ~30-MG hot-spot field for a predicted hot-spot radius of 17 μm. The deflection of the first peak can be used to estimate a residual magnetic field in the shell of 0.8 MG averaged over the shell thickness. The error in the magnetic field measurement comes from two sources, the error in the deflection (0.1 cm) and the error in the hot-spot radius. The statistical error of the hot-spot radius can be estimated by looking at the total number of measured protons that pass through the core and shell, which is constrained by the GEANT4 fit to the data. An 0.5-mm section of a 17-μm radius core will have ~400 protons in the peak with the largest deflection resulting in an error of 5% for the core size. The measured magnetic field is 30 ± 2 MG. The shell is estimated to be 70 μm in diameter and the first peak (smallest deflection) will have ~1300 protons in a lineout 0.5 mm wide for an error of 3% in the shell size. The magnetic field in the shell is 0.8 ± 0.1 MG.

When the seed field direction was reversed (via reversal of the current in the coils), the deflection pattern [Fig. 5(b), shot 52532] reversed direction, with the deflection now away from the target stalk (a spatial reference fixed for all shots). This confirms the magnetic nature of the deflection and supports the "relocation" of the high-field deflection to the other side of the core. This is also evident in lineouts at several energies shown in Fig. 5(b), where in addition to the offset peak near the center, there is again a concentration of tracks away from it (at -1.9 cm), caused by the peak of the compressed field in the hot spot. Analysis of the peak deflection revealed that the higher seed field (-62 kG) for this shot was amplified to at least -36 ± 3 MG. The larger peak area for Fig. 5(b) suggests higher hot-spot uniformity as more protons fall into these energy bands after being slowed down. The fields determined from Figs. 5(a) and 5(b) are the most conservative values, given by the lowest field B max, spread over the largest radius R_B, that can result in the observed deflection $\theta \sim \langle R_B B_{\max} \rangle$ without violating the flux conservation condition $\Phi \sim \langle R_B^2 B_{\max} \rangle \leq \Phi_0$. If the more realistic case is con-

TABLE I. Collision (ν_{ie}, ν_{ii}), gyrofrequencies (ω_{ci}), Hall parameter, and Larmor radii for a simulated cylindrical magnetized hot spot ($R = 18$ μm) with an average field of 30 MG.

ν_{ie} ns^{-1}	ν_{ii} ns^{-1}	ω_{ci}/ν_{ii}	mfp$_{ie}$ μm	mfp$_{ii}$ μm	r_L, μm
5.4	147	0.97	151	5.6	5.7

sidered, where up to 40% of the initial magnetic flux ($\Phi_0 \approx 360\,\mathrm{G\,cm^2}$) is lost as predicted by the hydro simulation, the estimated magnetic fields need to be revised upward to match the observed deflections.

The effect of the amplified magnetic field on the neutron yields was expected to be rather small for this experimental configuration even if the 1-D hydrocode predicts 2 to 3× increase in the yield caused by the temperature increase from thermal insulation in the hot spot. In the magnetized hot spot, the hydrocode did not correctly predict the fusion rate since the hot-spot size is such that the hot ions most likely to undergo fusion reactions (at the Gamow peak) are in the kinetic regime with their mean free path comparable to the hot-spot radius. This can be seen from Table I, where $n_{e,\mathrm{hs}} = 8 \times 10^{22}$ cm^{-3}, $T_{\mathrm{hs}} = 1.5$ keV, the Gamow peak is at 8.2 keV, and the Coulomb logarithms for the collisions of the 8-keV ions with thermal electrons and ions are $\Lambda_{ie} \approx 5$ and $\Lambda_{ii} \approx 8.6$, respectively. It is clear that the ions, having an ~6-μm mean free path, will undergo only a few collisions before leaving the hot spot. The electrons are fully magnetized but are thermally decoupled from the ions since the thermal equilibration time is of the order of 100 ps. Note that the higher temperatures are accompanied by lower hot-spot densities (Fig. 6) and lower plasma pressures since the total pressure (plasma + magnetic) is approximately independent of the magnetic field (the minimum volume-averaged hot-spot beta is ~300, but is of the order of unity in the center).

The highest neutron yield of 5.8×10^8 was measured in shot 49704 with a 10-kG seed field. With the present setup, however, caused by target parameter variations (gas pressure, orientation, positioning, and build quality), the $B_0 = 0$ yields already have variations of more than a factor of 3 (between 7.7×10^7 and 4.5×10^8). Such large shot-to-shot variations prevent an accurate assessment of the B-field effects on the fusion yield. The situation should improve in planned spherical magnetized implosions where the hot-spot density and collisionality are significantly higher and the experimental setup will exhibit greater repeatability.

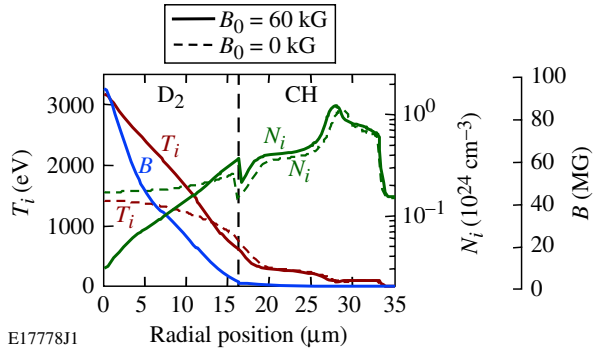

FIG. 6 (color online). LILAC-MHD simulations show drop in the hot-spot density and a temperature increase caused by the magnetic field. The compressed magnetic field profile is shown as the solid blue curve. Hot-spot temperature is plotted as red curves and hot-spot density is plotted as green curves. Temperature and density profiles with (without) the magnetic field are plotted as solid (dashed) lines.

In summary, very high magnetic-flux compression has been achieved using the ablative pressure of the OMEGA laser to drive a cylindrical shell at high implosion velocity, trapping and compressing the embedded external field to tens of MG, high enough to magnetize the hot-spot plasma. Finding the parameter space where the target performance will be most affected by the compressed magnetic is the next step in these studies.

The authors would like to thank Dr. F. Y. Thio and Dr. A. Velikovich for many illuminating discussions and for their encouragement in pursuing these novel experiments. This work was supported by the U.S. Department of Energy under Grant No. DE-FG02-04ER54768 and Cooperative Agreement Nos. DE-FC02-ER54789 and DE-FC52-08NA28302, the University of Rochester, and the New York State Energy Research and Development Authority.

[1] J. A. Wesson, *Tokamaks* (Clarendon Press, Oxford, 2004), 3rd ed.; A. H. Boozer, Rev. Mod. Phys. **76**, 1071 (2005).
[2] R. C. Kirkpatrick, I. R. Lindemuth, and M. S. Ward, Fusion Technol. **27**, 201 (1995).
[3] R. Betti *et al.*, Plasma Phys. Controlled Fusion **48**, B153 (2006).
[4] P. W. McKenty *et al.*, Phys. Plasmas **8**, 2315 (2001).
[5] J. A. Stamper, Laser Part. Beams **9**, 841 (1991).
[6] F. Herlach, Rep. Prog. Phys. **31**, 341 (1968); F. Herlach, Rep. Prog. Phys. **62**, 859 (1999).
[7] C. M. Fowler, W. B. Garn, and R. S. Caird, J. Appl. Phys. **31**, 588 (1960).
[8] A. D. Sakharov, Sov. Phys. Usp. **9**, 294 (1966).
[9] F. S. Felber, M. A. Liberman, and A. L. Velikovich, Phys. Fluids **31**, 3675 (1988); F. S. Felber *et al.*, J. Appl. Phys. **64**, 3831 (1988).
[10] O. V. Gotchev *et al.*, J. Fusion Energy **27**, 25 (2008).
[11] M. A. Liberman and A. L. Velikovich, J. Plasma Phys. **31**, 381 (1984).
[12] A. Hasegawa *et al.*, Phys. Rev. Lett. **56**, 139 (1986).
[13] T. R. Boehly *et al.*, Opt. Commun. **133**, 495 (1997).
[14] O. V. Gotchev *et al.*, Rev. Sci. Instrum. **80**, 043504 (2009).
[15] C. K. Li *et al.*, Rev. Sci. Instrum. **77**, 10E725 (2006).
[16] J. R. Rygg *et al.*, Science **319**, 1223 (2008).
[17] C. K. Li *et al.*, Phys. Rev. Lett. **100**, 225001 (2008).
[18] F. H. Séguin *et al.*, Rev. Sci. Instrum. **74**, 975 (2003).
[19] S. Agostinelli *et al.*, Nucl. Instrum. Methods Phys. Res., Sect. A **506**, 250 (2003).
[20] N. W. Jang *et al.*, Bull. Am. Phys. Soc. **51**, 144 (2006).